Chemical Science

ROYAL SOCIETY OF CHEMISTRY

EDGE ARTICLE

View Article Online
View Journal | View Issue

Check for updates

Cite this: *Chem. Sci.*, 2020, **11**, 9937

All publication charges for this article have been paid for by the Royal Society of Chemistry

Received 23rd July 2020
Accepted 28th August 2020

DOI: 10.1039/d0sc04036c

rsc.li/chemical-science

Bouncing off walls – widths of exit channels from shallow minima can dominate selectivity control†

Mengna Bai,‡[ab] Zhitao Feng,‡[b] Jun Li[a] and Dean J. Tantillo*[b]

A selectivity model based on the widths of pathways to competing products, rather than barrier heights, is formulated for the butadiene + allyl cation reaction. This model was arrived at *via* analysis of stationary points, intrinsic reaction coordinates, potential energy surface shapes and direct dynamics trajectories, all determined using quantum chemical methods.

Introduction

Reactions between butadienes and allyl cations have been studied extensively from both mechanistic and synthetic perspectives. Reactions of these two types of components can lead to 4-, 5-, 6- or 7-membered rings *via* concerted or stepwise (formal) (2 + 2)/[$_\pi$2 + $_\pi$2],[1,2] (2 + 3)/[$_\pi$2 + $_\pi$2],[3,4] (4 + 2)/[$_\pi$4 + $_\pi$2][5–9] (the so-called "ionic Diels–Alder reaction") or (4 + 3)/[$_\pi$4 + $_\pi$2][3,4,10–12] cycloaddition reactions, respectively (Scheme 1). Which products are observed can be influenced by which substituents are attached to each component and the environment in which the reaction is run. Here we reinvestigate the parent reaction of butadiene + allyl cation (in the gas phase and DMSO), adding results from density functional theory (DFT) calculations to Pascual-Teresa and Houk's previously reported HF and MP2 results,[13] and including an expanded view of the butadiene + allyl cation potential energy surface (PES). In addition, we have examined variational transition states (VTSs)[14] and subjected this reaction to *ab initio* molecular dynamics (AIMD) simulations, of both downhill and uphill varieties,[15] to assess whether or not non-statistical dynamic effects play a role in determining product selectivity.[16–19] Our results have led to the conclusion that the *widths of pathways to products can sometimes be more important than barrier heights*—an entropic effect that has often been overlooked but has potential utility in constructing useful models of selectivity and in designing new selective reactions.

Computational methods

The *Gaussian 09* software suite[20] was used for all DFT calculations. The geometries and frequencies of minima and transition-state structures (TSSs) were optimized at the B3LYP-D3/6-311+G(d,p),[21–25] M06-2X/6-311+G(d,p),[26–28] M06-2X/6-311G(d), and ωB97X-D/6-311G(d)[29] levels of theory. TSSs were defined as such by frequency calculations that predicted exactly one imaginary frequency,[30] while minima showed no imaginary frequencies. Molecular structures were visualized using *CYLview*.[31] Intrinsic reaction coordinate (IRC)[32–34] calculations were performed to confirm that minimum energy pathways (MEPs) connected TSSs to the reactants and the products indicated. To explore the effect of solvation, calculations were also performed with M06-2X/6-311G(d) and the PCM solvation model for DMSO.[35] In addition, single-point energies were computed at the CCSD(T)-F12a/AVDZ[36] level using the *MOLPRO* 2015 package.[37] As shown in Fig. 1, the relative energies of stationary points are similar among different levels. VTSs and associated reaction paths were determined using *Gaussrate*[38]/*Polyrate*[39] with application of

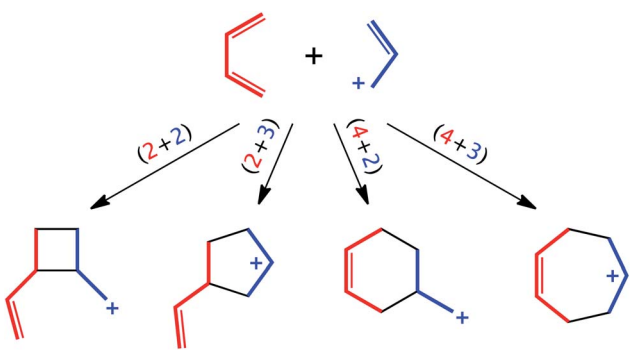

Scheme 1 Possible modes of cycloaddition for butadiene + allyl cation.

[a]*School of Chemistry and Chemical Engineering, Chongqing Key Laboratory of Theoretical and Computational Chemistry, Chongqing University, No. 55 Daxuecheng South Rd., Shapingba, Chongqing, 401331, China*

[b]*Department of Chemistry, University of California Davis, One Shields Avenue, Davis, CA 95616, USA. E-mail: djtantillo@ucdavis.edu*

† Electronic supplementary information (ESI) available: Additional details on computations, including coordinates and energies for computed structures and IRC plots (PDF). See DOI: 10.1039/d0sc04036c

‡ M. B. and Z. F. contributed equally.

Open Access Article. Published on 31 August 2020. Downloaded on 2/8/2026 4:19:01 PM.
This article is licensed under a Creative Commons Attribution-NonCommercial 3.0 Unported Licence.

Open Access Article. Published on 31 August 2020. Downloaded on 2/8/2026 4:19:01 PM.
This article is licensed under a Creative Commons Attribution-NonCommercial 3.0 Unported Licence.

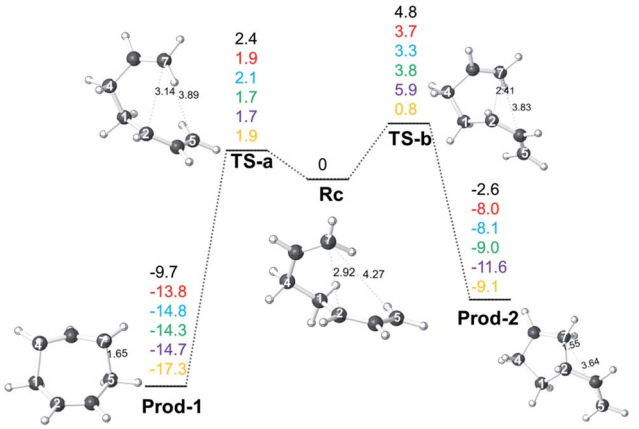

Fig. 1 Relative free energies (single point electronic energies for CCSD(T) results) of stationary points on the allyl cation + butadiene PES (in kcal mol^{-1} relative to **Rc**) at 298.15 K. The values shown are from top to bottom: B3LYP-D3/6-311+G (d,p) (black), M06-2X/6-311+G(d,p) (red), M06-2X/6-311G(d) (blue), ωB97X-D/6-311G(d) (green), PCM(DMSO)-M06-2X/6-311G(d) (purple), CCSD(T)-F12a/AVDZ//M06-2X/6-311G(d) (yellow). Distances shown (Å) are from structures optimized with M06-2X/6-311G(d). Structure labels are defined in the text below.

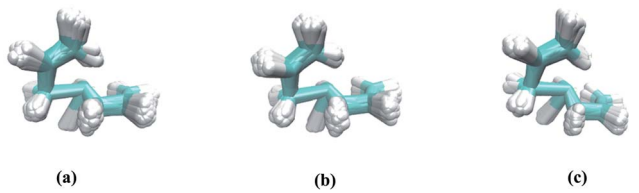

Fig. 2 Overlays of all starting geometries consistent with a Boltzmann distribution at 298 K in the region of **Rc**: (a) M06-2X/6-311G(d), (b) ωB97X-D/6-311G(d), (c) PCM(DMSO)-M06-2X/6-311G(d).

the Reorientation Of the Dividing Surface (RODS) algorithm at the M06-2X/6-311G(d) level of theory.[14,40]

Both quasi-classical and classical AIMD simulations were performed using M06-2X/6-311G(d). For the former, zero-point energies are included in initial sampling while for the latter, they are not. Quasi-classical AIMD simulations also were performed using ωB97X-D/6-311G(d). All trajectories were propagated using the *Progdyn*[41] script. To explore the effect of continuum solvent on dynamics, the PCM(DMSO)-M06-2X/6-311G(d) level of theory was employed. Uphill (initiated in the **Rc** region) and downhill (initiated in transition state regions) dynamics simulations were both carried out. For downhill dynamics, starting geometries were generated from a Boltzmann distribution of vibrations at 298 K and trajectories were propagated in both product and reactant directions with the Verlet algorithm, using *Gaussian 09* to calculate forces at each time step (the time step was set as 1 fs).[42] For uphill dynamics simulations, starting geometries were generated from a Boltzmann sampling of vibrations at 298 K then propagated towards the product direction until one or the other of the products is formed. Starting points for uphill dynamics are overlaid in Fig. 2. Note that our analysis here is for a "relaxed" **Rc**; *i.e.*, momentum for its formation is not included.[18,19] The following geometric criteria (atom numbers shown in Fig. 1) were employed to halt trajectories: when the C1–C4 and C5–C7 distances both dropped below 1.70 Å, a trajectory was labeled as the (4 + 3) adduct (7-membered ring product, **Prod-1**); when the C1–C4 and C2–C7 distances both dropped below 1.60 Å, a trajectory was labeled as the (2 + 3) adduct (5-membered ring product, **Prod-2**).

Results and discussion

Reaction coordinates

Energy profiles from different levels of theory for the allyl cation + butadiene reaction are shown in Fig. 1. No TSSs for concerted cycloaddition or formation of **Rc**, the product of addition of one end of the butadiene π-system to one end of the allyl π-system, were found; it appears that adduct formation is barrierless, at least in the absence of explicit solvent (appropriate modeling of which is beyond our current capabilities). This conclusion is consistent with previous studies on related reactions.[11c,12,13] Cation **Rc** can then be converted to 7- or 5-membered ring-containing products *via* concerted processes involving **TS-a** and **TS-b**, respectively. Note that the C=C group involved in bond formation (that which originated in the allyl fragment) rotates in opposite directions to form the 7- and 5-membered ring-containing products (*i.e.*, for an overall pathway connecting **Prod-1** to **Prod-2**, the migrating CH_2 group interacts antarafacially with the allyl group over which it migrates). While tempting to consider this observation a result of "vestiges of orbital symmetry,"[43] that cannot be done with confidence without more detailed examination of the PES preceding **Rc**. At all DFT levels of theory (but not CCSD(T), for which the data

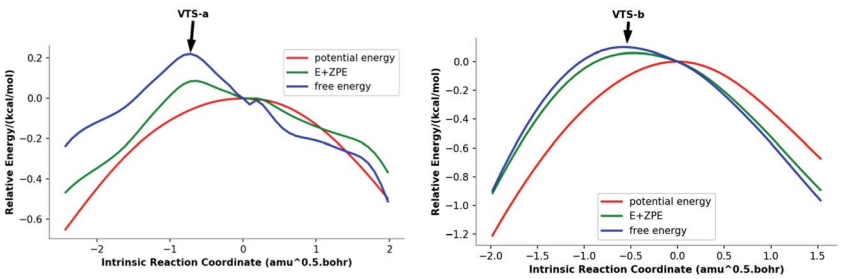

Fig. 3 Reaction coordinate plots (M06-2X/6-311G(d)) for pathways a (left) and b (right). The locations of **VTS-a** and **VTS-b** are highlighted.

This journal is © The Royal Society of Chemistry 2020

Open Access Article. Published on 31 August 2020. Downloaded on 2/8/2026 4:19:01 PM.
This article is licensed under a Creative Commons Attribution-NonCommercial 3.0 Unported Licence.

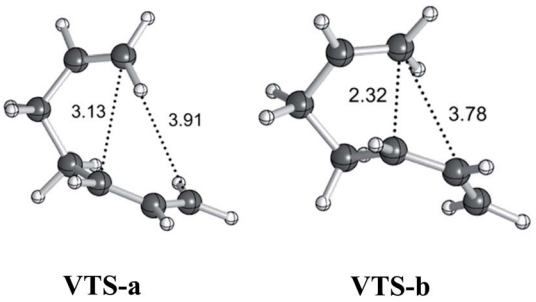

Fig. 4 Geometries (M06-2X/6-311G(d)) of variational transition states. Selected distances are shown in Å.

correspond to single-point electronic energies), **TS-b** is predicted to be higher in energy than **TS-a** and **Prod-2** was predicted to be higher in energy than **Prod-1**. Namely, in terms of either kinetic or thermodynamic control, formation of the 7-membered ring product, **Prod-1**, is favored. However, **Rc** is a shallow minimum, which can increase the lifetime and play a significant role in the dynamics, particularly at low temperatures.

Variational transition states

To address issues with standard computations of entropies, reaction pathways derived using variational transition state theory (VTST) calculations (using M06-2X/6-311G(d)) were computed; these are shown in Fig. 3. For both pathways, VTSs differ from the PES TSSs (compare the geometries of the VTSs in Fig. 4 with those of the TSSs in Fig. 1). The C5–C7 distance in **VTS-a** is 0.02 Å longer than that in **TS-a**, while the C2–C7 distance in **VTS-a** is 0.01 Å shorter than that in **TS-a**. The C5–C7 and C2–C7 distances in **VTS-b** are both shorter than those in **TS-b**, by 0.05 Å and 0.09 Å, respectively. Both VTSs are higher in free energy than the corresponding TSSs. As shown in Fig. 3, this effect is not simply an entropy effect, but also an effect of zero point energy. Note, however, that the difference in energy between the peaks of the free energy and potential energy curves is small—tenths of a kcal mol^{-1}—consistent with flat surfaces, in terms of both potential energy and free energy, near the transition states. No evidence for "entropic intermediates" is found here.[44,45]

Direct dynamics trajectories

Given the flatness of the PES near **Rc** and the transition states for cyclization, AIMD trajectory simulations were employed to evaluate (1) whether either transition state can lead to both products and (2) the factors influencing product selectivity.

Table 2 Results of downhill dynamics simulations initiated from VTSs (M06-2X/6-311G(d))

	Total trajectories	Trajectories that form product	Trajectories that recross
VTS-a	139	64	75
VTS-b	103	93	10

Downhill trajectories initiated from **TS-a** did in fact lead to both products, but just barely (Table 1), while trajectories initiated from **TS-b** did not. In both cases, however, a large amount of recrossing (here including trajectories connecting the reactant to the reactant, one product to the same product, or one product to the other product) was observed, consistent with a flat region of the PES.

Downhill trajectories were also initiated from **VTS-a** and **VTS-b**. Only **Prod-1** was formed from **VTS-a** and only **Prod-2** was formed from **VTS-b** (Table 2). While recrossing trajectories were much reduced for **VTS-b**, compared to **TS-b**, a high percentage of recrossing was still observed for **VTS-a**.

Results for uphill AIMD trajectories initiated at **Rc** are shown in Table 3. At all levels of theory, formation of the 7-membered ring-containing product, **Prod-1**, is much preferred. However, the predicted **Prod-1**/**Prod-2** ratio is lower than expected based on differences in TSS free energies (Fig. 1). For example, at ωB97-XD/6-311G(d), the ratio from dynamics simulation is 90 : 10, while that from free energy differences for TSSs is 97 : 3. As described above, VTS free energies differ only slightly from TSS free energies. With PCM(DMSO)-M06-2X/6-311G(d), free energy differences predict essentially no **Prod-2**, but our dynamics simulations predict that 16.5% of trajectories lead to this product. What is the origin of this discrepancy? Is it technical or chemical in nature?

Since our trajectories often involved thousands of fs to form products (see ESI†), we were concerned about ZPE leakage (generally a worry past ~0.5 ps).[46–49] To address this issue, we also carried out classical AIMD simulations. Results (using M06-2X/6-311G(d)) for uphill AIMD trajectories initiated at **Rc** and for downhill AIMD trajectories initiated at **VTS-a** are shown in Tables 4 and 5, respectively. For uphill simulations, the predicted **Prod-1**/**Prod-2** ratio does not change significantly between classical and quasi-classical simulations (compare Tables 3 and 4). For downhill simulations, a significantly smaller proportion of trajectories recrossed for classical *vs.* quasi-classical dynamics (compare Tables 2 and 5), but a large proportion of recrossing was still observed.

Table 1 Results of downhill dynamics simulations initiated from **TS-a** and **TS-b** (M06-2X/6-311G(d))

	Total trajectories	Trajectories that form **Prod-1**	Trajectories that form **Prod-2**	Trajectories that recross
TS-a	702	403	3	296
TS-b	699	0	451	248

Open Access Article. Published on 31 August 2020. Downloaded on 2/8/2026 4:19:01 PM.
This article is licensed under a Creative Commons Attribution-NonCommercial 3.0 Unported Licence.

Table 3 Results of uphill dynamics simulations initiated from **Rc**

Method	Total trajectories	Trajectories that form **Prod-1**	Trajectories that form **Prod-2**
M06-2X/6-311G(d)	206	171 (83%)	35 (17%)
ωB97X-D/6-311G(d)	154	138 (90%)	16 (10%)
PCM(DMSO)-M06-2X/6-311G(d)	91	76 (84%)	15 (16%)

Potential energy surfaces

To explore how shape of the PES influences the selectivity of the reaction, PESs for gas phase (M06-2X/6-311G(d)) and DMSO (PCM-M06-2X/6-311G(d)) reactions were built (Fig. 5) using relaxed scans along C5–C7 and C2–C7 distances (see Fig. 1 for atom labels) as *x*- and *y*-axes and energy displayed as height and color (top surfaces) or color alone (bottom surfaces, projections of top surfaces into the *x*–*y* plane). While these are reduced-dimension PESs, the geometric parameters used correspond to those of the forming bonds.[50,51] Small C5–C7 distances correspond to the **Prod-1** region, while small C2–C7 distances correspond to the **Prod-2** region. The locations of the two TSSs are marked, as are the IRC paths. One observation is immediately apparent from these surfaces: the pathway toward **Prod-1** is wider than the pathway toward **Prod-2**.

Representative gas phase trajectories are plotted in Fig. 6. As expected, long-time trajectories sample more of the **Rc** region on the PES before forming products. Importantly, some trajectories heading toward product "turn back" before crossing the dividing surface that separates reactant from products, *i.e.*, they miss the exit channel and instead "bounce off the wall" flanking it. This is distinct from recrossing, where the dividing surface is passed before a trajectory turns back (at least for the dimensions we have plotted here).[16–19] This is also distinct from bouncing off the side walls of a valley en route to product(s), *i.e.*, where deviations from an IRC still lead to product(s), not back to reactant(s).[16] The proportion of **Prod-1** forming trajectories that arose from "turning back" (62/171 or 36%) is larger than the proportion of **Prod-2** forming trajectories that arose from "turning back" (7/35 or 20%), *i.e.*, more **Prod-1** is formed from trajectories that initially miss the exit channel toward which they started, presumably because the exit channel toward **Prod-1** is wider. The product ratio predicted on the basis of "turn back" trajectories alone is 90 : 10 (62 *vs.* 7 trajectories). The ratio predicted on the basis of direct trajectories (here there are 137, making for a total of 206 as shown in Table 3) is 80 : 20, and the overall ratio accounting for all product-forming trajectories is 83 : 17 (Table 3). Thus, the ratio predicted from direct uphill trajectories does not reflect the predicted free energies of transition states, be they TSSs or VTSs, and the "turning back" phenomenon increases selectivity for the product formed *via*

Table 4 Classical dynamics results of uphill dynamics simulations initiated from **Rc** (M06-2X/6-311G(d))

	Total trajectories	Trajectories that form **Prod-1**	Trajectories that form **Prod-2**
Rc	90	75 (83%)	15 (17%)

Table 5 Classical dynamics results of downhill dynamics simulations initiated from **VTS-a** (M06-2X/6-311G(d))

	Total trajectories	Trajectories that form product	Trajectories that recross
VTS-a	130	91	39

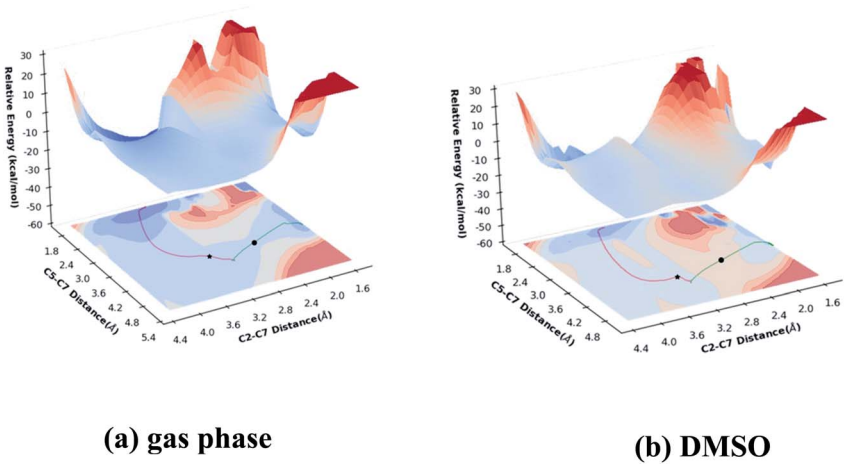

Fig. 5 Potential energy surfaces: (a) M06-2X/6-311G(d), (b) PCM(DMSO)-M06-2X/6-311G(d). IRCs for **TS-a** are shown as red lines and IRCs for **TS-b** are shown as green lines. **TS-a** and **TS-b** are indicated as stars and circles, respectively.

 This journal is © The Royal Society of Chemistry 2020

Open Access Article. Published on 31 August 2020. Downloaded on 2/8/2026 4:19:01 PM.
This article is licensed under a Creative Commons Attribution-NonCommercial 3.0 Unported Licence.

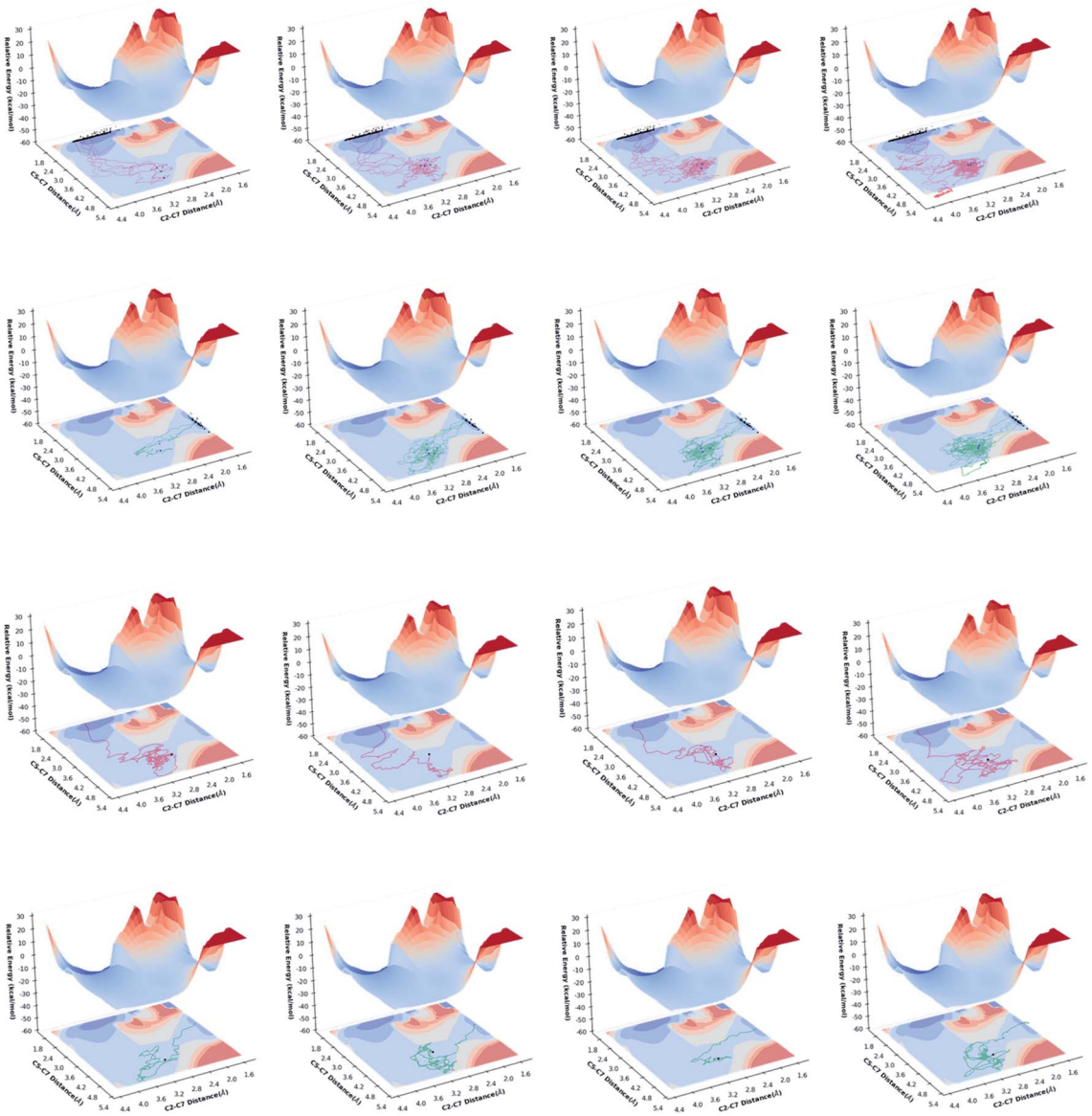

Fig. 6 (1) Projections of trajectories onto the M06-2X/6-311G(d) PES, based on trajectory length (time). Left to right: 0–500 fs, 500–1000 fs, 1000–1500 fs, 1500–2000 fs. The first row corresponds to **Prod-1**-forming trajectories. The second row corresponds to **Prod-2**-forming trajectories. (2) Projections of representative "turn back" trajectories onto the M06-2X/6-311G(d) PES. The third row shows representative **Prod-1**-forming "turn back" trajectories. The bottom row shows representative **Prod-2**-forming "turn back" trajectories.

the wider pathway. A similar effect was recently discussed for a different carbocation reaction, but from the perspective of downhill trajectories and post-transition state bifurcations.[52]

A close-up view of the reactant region of the PES is shown in Fig. 7, which also shows the locations of the VTSs. **TS-a** and **VTS-a** occupy similar positions in this plot, consistent with similar amounts of recrossing in downhill AIMD. **VTS-b** is noticeably later (closer to product in terms of the geometric parameters plotted here) than is **TS-b**, consistent with reduced recrossing. Being later, it is further into the least wide region of the path to products, consistent with it being even more difficult for uphill trajectories to reach **Prod-2** than if they only had to reach **TS-b**. This region of decreased width indicates that varying the C5–C7 distance happens to be particularly difficult near the transition state for formation of the C2–C7 bond. This phenomenon was unexpected, but is perhaps related to the fact that the forming σ-bond is much shorter in

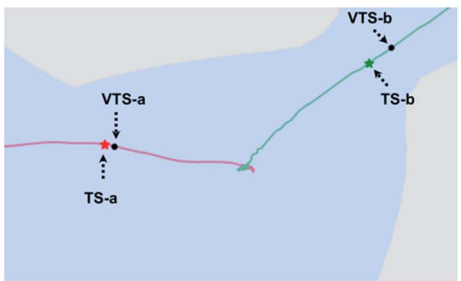

Fig. 7 Close-up view of the reactant region of the surface from Fig. 5a.

Open Access Article. Published on 31 August 2020. Downloaded on 2/8/2026 4:19:01 PM. This article is licensed under a Creative Commons Attribution-NonCommercial 3.0 Unported Licence.

TS-b and **VTS-b** than in **TS-a** and **VTS-a** and conformational restrictions due to hyperconjugation with the forming σ-bond are expected, therefore, to be more severe.

This pathway width effect is clearly connected to entropy, *i.e.*, a wider path is related to more flexibility and more possible ways to cross through a dividing surface.[40,45,53–55] This effect appears not to be captured fully in VTS free energies, however, at least for the system examined here, which involves a flat energy surface, although we cannot definitively rule out the possibility that the apparent discrepancy is due to the particulars of running each type of calculation. Nonetheless, interpreting results of this type in terms of pathway widths allows one to better tie specific structural features to entropy changes along reaction coordinates.

Conclusions

We have explored the mechanism of the reaction between butadiene and allyl cation using quantum chemical computations on PESs and direct AIMD simulations (quasi-classical and classical). Consistent with results from previous calculations at other levels of theory,[13] concerted cycloaddition pathways are not found. Instead, stepwise pathways leading to products of formal (4 + 3) and (2 + 3) cycloaddition are present, but these involve a shallow intermediate with low barrier exit channels. As for other reactions with shallow intermediates—twixtyls, calderas, mesas, para-intermediates[19,56–58]—non-traditional effects appear to play a key role in product formation. We propose that the product selectivity in the system examined here—and likely others[52]—is determined by dynamic effects related to the *width* of pathways to products. In particular, there is an entropy effect—transition states with wider energy wells orthogonal to the reaction coordinate have more possible paths through them—which is modulated, enhanced in this case, by an unequal probability of trajectories turning back before reaching transition states. We are currently expanding on this work to see if models based on pathway width can rationalize product selectivity for cases with existing experimental evidence for entropy-controlled selectivity where the origins of that entropy control are not known.

Conflicts of interest

The authors declare no competing financial interest.

Acknowledgements

Support from the National Science Foundation (CHE-1856416 and supercomputing resources from the XSEDE program *via* CHE-030089) and the National Natural Science Foundation of China (contract no. 21573027 and 21973009) is gratefully acknowledged. Mengna Bai thanks the fund from the China Scholarship Council (CSC).

References

1 Y. J. Hong and D. J. Tantillo, How Cyclobutanes are Assembled in Nature - Insights from Quantum Chemistry, *Chem. Soc. Rev.*, 2014, **43**, 5042–5050.
2 P. G. Gassman and A. C. Lottes, Cyclobutane Formation in the 2π+2π Cycloaddition of Allyl and Related Cations to Unactivated Olefins. Evidence for the 2nd Step in the Proposed Mechanism of the Ionic Diels-Alder Reaction, *Tetrahedron Lett.*, 1992, **33**, 157–160.
3 H. M. R. Hoffmann, The Cycloaddition of Allyl Cations to 1,3-Dienes - General-Method for the Synthesis of 7-Membered Carbocycles, *Angew. Chem. Int. Ed.*, 1984, **23**, 1–19.
4 H. M. Hoffmann, Syntheses of 7-Membered and 5-Membered Rings from Allyl Cations, *Angew. Chem. Int. Ed.*, 1973, **12**, 819–835.
5 R. K. Haynes, G. R. King and S. C. Vonwiller, Preparation of a Bicyclic Analog of Qinghao (Artemisinic) Acid via a Lewis-Acid Catalyzed Ionic Diels-Alder Reaction Involving a Hydroxy Diene and Cyclic Enone and Facile Conversion into (+/-)-6,9-Desdimethylqinghaosu, *J. Org. Chem.*, 1994, **59**, 4743–4748.
6 P. G. Gassman and D. B. Gorman, Stepwise Mechanism for the Formation of 2π+ 4π Cycloadducts in the Ionic Diels-Alder Reaction, *J. Am. Chem. Soc.*, 1990, **112**, 8624–8626.
7 P. G. Gassman and D. A. Singleton, Acid-Catalyzed Intramolecular Diels-Alder Reactions - the Cycloaddition of Allyl Cations to 1,3-Dienes, *J. Am. Chem. Soc.*, 1984, **106**, 6085–6086.
8 P. G. Gassman, D. A. Singleton, J. J. Wilwerding and S. P. Chavan, Acrolein Acetals as Allyl Cation Precursors in the Ionic Diels-Alder Reaction, *J. Am. Chem. Soc.*, 1987, **109**, 2182–2184.
9 Y. J. Ko, S. B. Shim and J. H. Shin, A Mechanistic Study on the Intramolecular Ionic Diels-Alder Reaction of 2-Methyl-3,9,11-Tridecatriene-2-ol and 2,11-Dimethyl-1,3,9,11-Dodecatetraene, *Tetrahedron Lett.*, 2007, **48**, 863–867.
10 R. B. Woodward and R. Hoffmann, *The Conservation of Orbital Symmetry*, Elsevier, 2013.
11 (*a*) M. Harmata, The (4+3)-Cycloaddition Reaction: Simple Allylic Cations as Dienophiles, *Chem. Commun*, 2010, **46**, 8886–8903; (*b*) M. Harmata, Intramolecular Cycloaddition Reactions of Allylic Cations, *Tetrahedron*, 1997, **53**, 6235–6280; (*c*) M. Harmata and P. R. Schreiner, Intramolecular 4 + 3 Cycloadditions. A Theoretical Analysis of Simple Diastereoselectivity in Reactions of Alkoxyallylic Cations and Furans, *Org. Lett.*, 2001, **3**, 3663–3665.
12 C. J. Cramer and S. E. Barrows, Quantum chemical characterization of cycloaddition reactions between 1,3-butadiene and oxyallyl cations of varying electrophilicity, *J. Phys. Org. Chem.*, 2000, **13**, 176–186.
13 B. de Pascual Teresa and K. N. Houk, The Ionic Diels-Alder Reaction of the Allyl Cation and Butadiene: Theoretical Investigation of the Mechanism, *Tetrahedron Lett.*, 1996, **37**, 1759–1762.
14 J. L. Bao and D. G. Truhlar, Variational Transition State Theory: Theoretical Framework and Recent Developments., *Chem. Soc. Rev.*, 2017, **46**, 7548–7596.
15 R. Pradhan and U. Lourderaj, Can Reactions Follow Non-Traditional Second-Order Saddle Pathways Avoiding Transition States?, *Phys. Chem. Chem. Phys.*, 2019, **21**, 12837–12842.

 This journal is © The Royal Society of Chemistry 2020

Open Access Article. Published on 31 August 2020. Downloaded on 2/8/2026 4:19:01 PM. This article is licensed under a Creative Commons Attribution-NonCommercial 3.0 Unported Licence.

16 X. Y. Ma and W. L. Hase, Perspective: Chemical Dynamics Simulations of Non-Statistical Reaction Dynamics, *Philos. Trans. R. Soc., A*, 2017, **375**, 20160204.
17 U. Lourderaj, K. Park and W. L. Hase, Classical Trajectory Simulations of Post-Transition State Dynamics, *Int. Rev. Phys. Chem.*, 2008, **27**, 361–403.
18 B. K. Carpenter, Intramolecular Dynamics for the Organic Chemist, *Acc. Chem. Res.*, 1992, **25**, 520–528.
19 B. K. Carpenter, Nonstatistical Dynamics in Thermal Reactions of Polyatomic Molecules, in *Ann. Rev. Phys. Chem.; Annual Review of Physical Chemistry*, Annual Reviews, Palo Alto, 2005, vol. 56, pp. 57–89.
20 M. J. T. Frisch, G. W. Trucks, H. B. Schlegel, G. E. Scuseria, M. A. Robb, J. R. Cheeseman, G. Scalmani, V. Barone, B. Mennucci, G. A. Petersson, H. Nakatsuji, M. Caricato, X. Li, H. P. Hratchian, A. F. Izmaylov, J. Bloino, G. Zheng, J. L. Sonnenberg, M. Hada, M. Ehara, K. Toyota, R. Fukuda, J. Hasegawa, M. Ishida, T. Nakajima, Y. Honda, O. Kitao, H. Nakai, T. Vreven, J. A. Montgomery Jr, J. E. Peralta, F. Ogliaro, M. Bearpark, J. J. Heyd, E. Brothers, K. N. Kudin, V. N. Staroverov, R. Kobayashi, J. Normand, K. Raghavachari, A. Rendell, J. C. Burant, S. S. Iyengar, J. Tomasi, M. Cossi, N. Rega, J. M. Millam, M. Klene, J. E. Knox, J. B. Cross, V. Bakken, C. Adamo, J. Jaramillo, R. Gomperts, R. E. Stratmann, O. Yazyev, A. J. Austin, R. Cammi, C. Pomelli, J. W. Ochterski, R. L. Martin, K. Morokuma, V. G. Zakrzewski, G. A. Voth, P. Salvador, J. J. Dannenberg, S. Dapprich, A. D. Daniels, Ö Farkas, J. B. Foresman, J. V. Ortiz, J. Cioslowski and D. J. Fox, *Gaussian 09*, Gaussian Inc., Wallingford, CT, 2009.
21 A. D. Becke, A New Mixing of Hartree-Fock and Local Density-Functional Theories, *J. Chem. Phys.*, 1993, **98**, 1372–1377.
22 A. D. Becke, Density-Functional Thermochemistry .3. The Role of exact Exchange, *J. Chem. Phys.*, 1993, **98**, 5648–5652.
23 C. T. Lee, W. T. Yang and R. G. Parr, Development of the Colle-Salvetti Correlation-Energy Formula into a Functional of the Electron-Density, *Phys. Rev. B: Condens. Matter Mater. Phys.*, 1988, **37**, 785–789.
24 P. J. Stephens, F. J. Devlin, C. F. Chabalowski and M. J. Frisch, Ab-Initio Calculation of Vibrational Absorption and Circular-Dichroism Spectra Using Density-Functional Force-Fields, *J. Phys. Chem.*, 1994, **98**, 11623–11627.
25 J. Tirado-Rives and W. L. Jorgensen, Performance of B3LYP Density Functional Methods for a Large Set of Organic Molecules, *J. Chem. Theory Comput.*, 2008, **4**, 297–306.
26 Y. Zhao and D. G. Truhlar, The M06 Suite of Density Functionals for Main Group Thermochemistry, Thermochemical Kinetics, Noncovalent Interactions, Excited States, and Transition Elements: Two New Functionals and Systematic Testing of Four M06-Class Functionals and 12 other Functionals, *Theor. Chem. Acc.*, 2008, **120**, 215–241.
27 Y. Zhao and D. G. Truhlar, Density Functionals with Broad Applicability in Chemistry, *Acc. Chem. Res.*, 2008, **41**, 157–167.
28 N. Mardirossian and M. Head-Gordon, How Accurate Are the Minnesota Density Functionals for Noncovalent Interactions, Isomerization Energies, Thermochemistry, and Barrier Heights Involving Molecules Composed of Main-Group Elements?, *J. Chem. Theory Comput.*, 2016, **12**, 4303–4325.
29 A. Sengupta and K. Raghavachari, Solving the Density Functional Conundrum: Elimination of Systematic Errors to Derive Accurate Reaction Enthalpies of Complex Organic Reactions, *Org. Lett.*, 2017, **19**, 2576–2579.
30 D. J. Tantillo, Biosynthesis via Carbocations: Theoretical Studies on Terpene Formation, *Nat. Prod. Rep.*, 2011, **28**, 1035–1053.
31 C. Y. Legault, *CYLview, 1.0b*, Université de Sherbrooke, 2009.
32 C. Gonzalez and H. B. Schlegel, Reaction-Path Following in Mass-Weighted Internal Coordinates, *J. Phys. Chem.*, 1990, **94**, 5523–5527.
33 K. Fukui, The Path of Chemical-Reactions - the IRC Approach, *Acc. Chem. Res.*, 1981, **14**, 363–368.
34 S. Maeda, Y. Harabuchi, Y. Ono, T. Taketsugu and K. Morokuma, Intrinsic Reaction Coordinate: Calculation, Bifurcation, and Automated Search, *Int. J. Quant. Chem.*, 2015, **115**, 258–269.
35 A. V. Marenich, C. J. Cramer and D. G. Truhlar, Universal Solvation Model Based on Solute Electron Density and on a Continuum Model of the Solvent Defined by the Bulk Dielectric Constant and Atomic Surface Tensions, *J. Phys. Chem. B*, 2009, **113**, 6378–6396.
36 L. G. Kong, F. A. Bischoff and E. F. Valeev, Explicitly Correlated R12/F12 Methods for Electronic Structure, *Chem. Rev.*, 2012, **112**, 75–107.
37 H. J. Werner, P. J. Knowles, G. Knizia, F. R. Manby and M. Schutz, Molpro: a General-Purpose Quantum Chemistry Program Package. WIREs, *Comput. Mol. Biosci.*, 2012, **2**, 242–253.
38 J. Zheng, S. Zhang, J. C. Corchado, Y.-Y. Chuang, E. L. Coitino, B. A. Ellingson and D. G. Truhlar, *GAUSSRATE, version 2009-A*, University of Minnesota, Minneapolis, MN, 2010.
39 J. Zheng, *et al*, *POLYRATE-version 2010*, University of Minnesota, Minneapolis, MN, 2010.
40 A. Gonzalez-Lafont, J. Villa, J. M. Lluch, J. Bertran, R. Steckler and D. G. Truhlar, Variational Transition State Theory and Tunneling Calculations with Reorientation of the Generalized Transition States for Methyl Cation Transfer, *J. Phys. Chem. A*, 1998, **102**, 3420–3428.
41 B. R. Ussing, C. Hang and D. A. Singleton, Dynamic Effects on the Periselectivity, Rate, Isotope Effects, and Mechanism of Cycloadditions of Ketenes with Cyclopentadiene, *J. Am. Chem.Soc.*, 2006, **128**, 7594–7607.
42 D. Marx and J. Hutter, *Ab initio molecular dynamics: basic theory and advanced methods*, Cambridge University Press, 2009.
43 A. G. Leach, S. Catak and K. N. Houk, Mechanism of the Forbidden 3s,5s-Sigmatropic Shift: Orbital Symmetry Influences Stepwise Mechanisms Involving Diradical Intermediates, *Chem.–Eur. J.*, 2002, **8**, 1290–1299.

Open Access Article. Published on 31 August 2020. Downloaded on 2/8/2026 4:19:01 PM.
This article is licensed under a Creative Commons Attribution-NonCommercial 3.0 Unported Licence.

44 Z. Y. Yang, C. S. Jamieson, X. S. Xue, M. Garcia-Borras, T. Benton, X. F. Dong, F. Liu and K. N. Houk, Mechanisms and Dynamics of Reactions Involving Entropic Intermediates, *Trends Chem.*, 2019, **1**, 22–34.

45 O. M. Gonzalez-James, E. E. Kwan and D. A. Singleton, Entropic Intermediates and Hidden Rate-Limiting Steps in Seemingly Concerted Cycloadditions. Observation, Prediction, and Origin of an Isotope Effect on Recrossing, *J. Am. Chem. Soc.*, 2012, **134**, 1914–1917.

46 L. Bonnet and J. C. Rayez, Quasiclassical Trajectory Method for Molecular Scattering Processes: Necessity of a Weighted Binning Approach, *Chem. Phys. Lett.*, 1997, **277**, 183–190.

47 C. Doubleday, M. Boguslav, C. Howell, S. D. Korotkin and D. Shaked, Trajectory Calculations for Bergman Cyclization Predict H/D Kinetic Isotope Effects Due to Nonstatistical Dynamics in the Product, *J. Am. Chem. Soc.*, 2016, **138**, 7476–7479.

48 M. Bennun and R. D. Levine, Conservation of Zero-point Energy in Classical Trajectory Computations by a Simple Semiclassical Correspondence, *J. Chem. Phys.*, 1994, **101**, 8768–8783.

49 M. C. Reis, C. S. Lopez, O. N. Faza and D. J. Tantillo, Pushing the Limits of Concertedness. A Waltz of Wandering Carbocations, *Chem. Sci.*, 2019, **10**, 2159–2170.

50 H.-H. Chuang, D. J. Tantillo and C.-P. Hsu, Construction of Two-Dimensional Potential Energy Surfaces of Reactions with Post-Transition-State Bifurcations, *J. Chem. Theory Comput.*, 2020, **16**, 4050–4060.

51 B. K. Carpenter, Understanding Chemical Reaction Mechanisms, in *Of Minds and Molecules*, ed. N. Bhushan and S. Rosenfeld, Oxford University Press New York, 2000, pp. 223–224.

52 S. R. Hare, R. P. Pemberton and D. J. Tantillo, Navigating Past a Fork in the Road: Carbocation-π Interactions Can Manipulate Dynamic Behavior of Reactions Facing Post-Transition-State Bifurcations, *J. Am. Chem. Soc.*, 2017, **139**, 7485–7493.

53 (*a*) E. V. Anslyn and D. A. Dougherty, *Modern Physical Organic Chemistry*, University Science Books, Sausalito, 2006, vol. 369, pp. 412–413; (*b*) C. Stegelmann, A. Andreasen and C. T. Campbell, Degree of Rate Control: How Much the Energies of Intermediates and Transition States Control Rates, *J. Am. Chem. Soc.*, 2009, **131**, 8077–8082.

54 Z. H. Wang, J. S. Hirschi and D. A. Singleton, Recrossing and Dynamic Matching Effects on Selectivity in a Diels-Alder Reaction, *Angew. Chem. Int. Ed.*, 2009, **48**, 9156–9159.

55 J. N. Harvey, Understanding the Kinetics of Spin-forbidden Chemical Reactions, *Phys. Chem. Chem. Phys.*, 2007, **9**, 331–343.

56 R. Hoffmann, S. Swaminathan, B. G. Odell and R. Gleiter, Potential Surface for a Nonconcerted Reaction-Tetramethylene, *J. Am. Chem. Soc.*, 1970, **92**, 7091–7097.

57 W. V. Doering, J. L. Ekmanis, K. D. Belfield, F. G. Klarner and B. Krawczyk, Thermal Reactions of Anti- and Syn-Dispiro 5.0.5.2 Tetradeca-1,8-Dienes: Stereomutation and Fragmentation to 3-Methylenecyclohexenes. Entropy-Dictated Product Ratios from Diradical Intermediates?, *J. Am. Chem. Soc.*, 2001, **123**, 5532–5541.

58 B. H. Northrop, D. P. O'Malley, A. L. Zografos, P. S. Baran and K. N. Houk, Mechanism of the Vinylcyclobutane Rearrangement of Sceptrin to Ageliferin and Nagelamide E., *Angew. Chem. Int. Ed.*, 2006, **45**, 4126–4130.

This journal is © The Royal Society of Chemistry 2020